The Classification for Steel Corroded Reinforced Concrete Beams Using Linear Discriminant Analysis

Ahmad Zaki[1], Zainah Ibrahim[2], Yessi Jusman[3]
{ahmad.zaki@umy.ac.id[1]}

Department of Civil Engineering, Faculty of Engineering, Universitas Muhammadiyah Yogyakarta, 55183 Yogyakarta, Indonesia[1]
Department of Civil Engineering, Faculty of Engineering, University of Malaya, 50603 Kuala Lumpur, Malaysia[2]
Department of Electrical Engineering, Faculty of Engineering, Universitas Muhammadiyah Yogyakarta, 55183 Yogyakarta, Indonesia[3]

Abstract. Corrosion of steel reinforcement in the reinforced concrete (RC) members contribute to structural damage and failure. This study proposes a damage classification method for corroded reinforced concrete (RC) beams subjected to flexural loading by linear discriminant analysis (LDA) of acoustic emission (AE) data. The structural behavior of RC beam specimens induced with varying steel corrosion levels was evaluated by AE monitoring during the flexural load test. Analysis of primary AE data, RA value (ratio of rise time to amplitude of the waveforms) could be correlated and used to classify the fracture type. It was found that the proposed LDA could achieve good accuracy in damage classification of corroded RC beams.

Keywords: Corrosion, concrete, AE technique, LDA

1 Introduction

Corrosion of the steel reinforcements in RC structures is a worldwide problem [1]. The corrosion has been recognized as the major deterioration mechanism which affects RC degradation due to the environmental actions [2]. The costs of repair and maintenance of corroded structures worldwide exceed billions of dollars per year [3]-[6]. It becomes necessary that the effects of steel reinforcement corrosion on RC structures' functionality be detected early and studied in detail using an effective inspection method to provide effective remedial means [7]-[9]. Non-destructive testing (NDT) method is an objective-oriented inspection method for damage evaluations, i.e., steel corrosion [9]-[13]. Regarded as one of the popular NDT methods based on elastic wave propagation monitoring, the Acoustic Emission (AE) technique has also been studied for use in detecting steel corrosion in concrete [14]-[16]. The elastic waves generated due to corrosion events (i.e., cracking) could be successfully detected by placing AE sensors on the surface of concrete [17]-[19]. The first recorded application of the AE technique for corrosion evaluation in RC structure was done by Dunn et al. in 1984 [20]. The AE parameters, such as accumulated hits, signal strength, and energy, were successfully used to identify and characterize the RC structures' steel corrosion. The AE sources were also classified in terms of RA value and AF to classify the type of failure [21]-[24].

Many classification techniques for interpreting AE data have been developed in recent years. However, to date, success has been limited to interpreting the AE data. Therefore, this

BIS-HSS 2020, November 18, Indonesia

DOI 10.4108/eai.18-11-2020.2311755

research aims to represent classification techniques in a suitable format that evaluates the steel corroded of the concrete structure. In this study, mechanical load testing was conducted at several RC beams with varying corrosion levels through recorded data of the AE activity to classify the damage by linear discriminant analysis (LDA). The AE parameters, namely RA value, were obtained to evaluate the corroded RC beams. Therefore, a drop in RA value could be indicative of an impending fracture. Thus, LDA was conducted to study the drop of RA value of the monitored AE data for corroded beam specimens' damage classification.

2 Method

2.1 Materials

Four concrete beam specimens with varying corrosion levels (i.e., Control (0%), 9.54%, 19.84%, and 24.60%) were prepared in the study. The corrosion levels of beam specimens were 0% for S0, 9.54% for S10, 19.84% for S20, and 24.60% for S25. The concrete beams have dimensions of length = 500 mm, width = 100 mm, and height = 100 mm. The diameter of the tensile reinforcement was 12 mm. The bottom cover was 26 mm from the concrete surface. The details of beam specimen are shown in Figure 1.

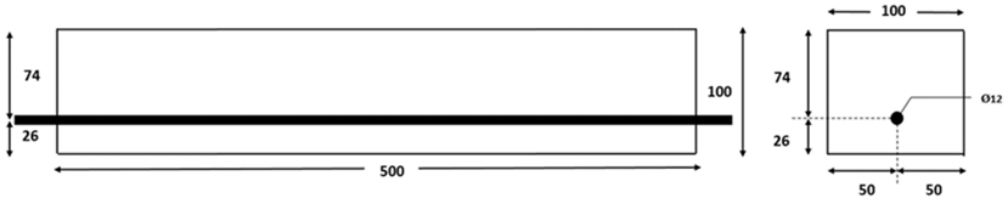

Fig. 1. Details of beam specimen (units are in mm)

Ordinary Portland cement (OPC), river sand, and crushed granite with a maximum aggregate size of 10 mm were used to prepare the concrete mixture. The compressive strength, average modulus of modulus elasticity, and average Poisson's ratio of the concrete at 28th day of after casting are 37,31 MPa, 26,49 GPa, and 0,17, respectively.

2.2 Accelerated corrosion technique

Corrosion was induced to the steel reinforcement using the impressed current technique after 28th days of moist curing, by adopting a direct current (DC) power supply [6, 25, 26]. The corrosion level was obtained from the voltage, current, and duration of exposure (time interval) using Faraday's Law [27].

$$\Delta m = \frac{M.I.t}{z.F} \tag{1}$$

Where: Δm = mass of steel consumed (g, gram), M = atomic or molecular weight of metal (56 g/mol for steel), I = current (A, amperes), t = time current or potentials applied (s, seconds), z = ionic charge or electrons transferred in the half-cell reaction (2 for steel) and F = Faraday's constant (96500 A/s).

The positive terminal of a DC power supply was connected to steel reinforcement as an anode by an electrical wire, while the negative terminal was connected to the steel reinforcement bar as a cathode. The concrete was partially immersed in a water tank filled with 5% sodium chloride (NaCl) solution. The NaCl solution was in contact with the bottom of the concrete beam. During the corrosion process, the electrical current was kept constant. The corrosion process was continuously monitored until the steel reinforcement corroded to the estimated mass loss required with different exposure times.

2.3 AE data acquisitions

During the load testing, the beam specimens were also monitored using the AE technique. For the AE data acquisition, six AE sensors were attached to each concrete specimen. The schematic acquisitions of the AE technique are shown in Figure 2.

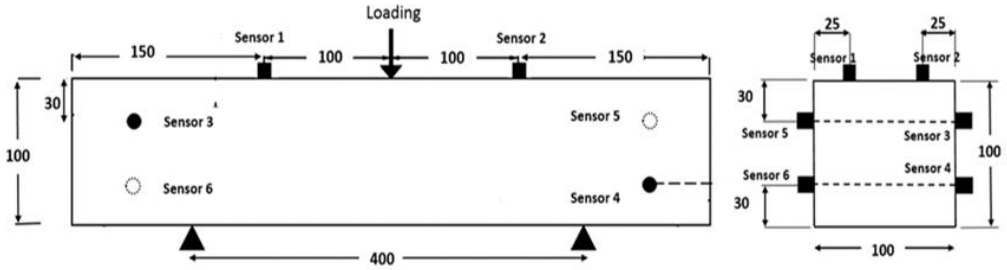

Fig 2. Schematic data acquisitions of AE technique (unit are in mm)

2.4 Linear discriminant analysis (LDA)

The LDA performs well in many applications. LDA's basic idea is simple: for each class to be identified, calculate a (different) linear function of the attributes. The class function yielding the highest score represents the predicted class. There are many linear classification models, and they are different largely in how the coefficients are established. LDA does not require multiple passes over the data for optimization. Also, it naturally handles problems with two classes and more. It can estimate the probability for each of the candidate classes [28].

The LDA solves a general Eigen-problem. Suppose there are C classes and n number of d-dimensional training samples, and nc denotes the number of training samples of class c. Let 1 denotes an all-one vector of proper length. The equations for within-class scatter matrix, Sw, between-class scatter matrix, Sb, and total scatter matrix, St, are:

$$S_w = \frac{1}{n}\sum_{c=1}^{C}\left(\hat{X}_c - m_c 1^T\right)\left(\hat{X}_c - m_c 1^T\right)^T S_w = \frac{1}{n}\sum_{c=1}^{C}\left(\hat{X}_c - m_c 1^T\right)\left(\hat{X}_c - m_c 1^T\right)^T \quad (2)$$

$$S_b = \frac{1}{n}\sum_{c=1}^{C} n_c (m_c - m)(m_c - m)^T S_b = \frac{1}{n}\sum_{c=1}^{C} n_c (m_c - m)(m_c - m)^T \quad (3)$$

$$S_t = \frac{1}{n}\left(\hat{X} - m1^T\right)\left(\hat{X} - m1^T\right)^T S_t = \frac{1}{n}\left(\hat{X} - m1^T\right)\left(\hat{X} - m1^T\right)^T \quad (4)$$

Where: $\hat{X} \in R^{dxn}$ = the data matrix in which the columns are training samples, $\hat{X}_c$ = the data matrix of training samples belonging to the class c, m = the mean vector of all training

samples, mc = the mean vector of training samples belonging to the class c, and T = denotes matrix transpose.

The LDA computes a linear transformation matrix W ∈ Rd×(C−1), and usually d ≫ C. The transformation matrix projects data from the original high-dimensional space into a low-dimensional space, maximizing the between-class distance while minimizing the within-class distance. Traditional LDA finds the optimal transformation matrix WLDA by solving the optimization problem [28].

$$W_{LDA} = arg_W \max trace(W^T S_b W (W^T S_t W)^{-1}) \tag{5}$$

According to Galloway [29], when the total scatter matrix St is non-singular, the solution WLDA consists of the top eigenvectors of the matrix (S_t^(-1) S_b) that corresponds to non-zero eigenvalues. When the total scatter matrix St does not have a full rank, WLDA consists of the eigenvectors of (S_t^+ S_b) corresponding to the non-zero eigenvalues S_t^+ denotes the pseudo-inverse of St [30].

3 Result and Discussion

3.1 Accumulated of AE hits

Figure 3 shows the relationship between the accumulated AE hits and load level (%) of the beam specimens. The accumulated AE hits decrease as the corrosion level of the specimens increases. In general, as the load is applied, the AE hits appear to increase before the first visible cracks. After forming the first visible crack at the range of 10% to 30% of the load level, AE hits' rate rapidly increases. Afterward, as the loading continues, the cracks propagate, and the AE hits gradually increase until beam specimen failure occurs. Based on the history of accumulated AE hits, the trend of the accumulated AE hits can provide useful information in evaluating the damage level of the corroded beam specimens. This trend may be attributed to the stressing and majority of cracking, especially longitudinal cracking along the steel reinforcement, which has already been dissipated by the steel corrosion.

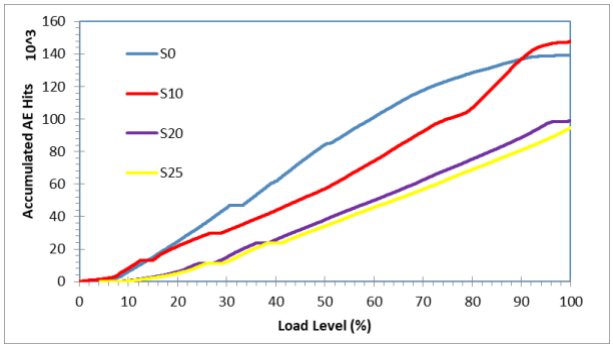

Fig 3. Accumulated AE hits versus load level (%) of beam specimens

The correlation between accumulated AE hits and ultimate peak load or ultimate strength is shown in Figure 4. A decrease in ultimate strength was linear with the decrease in accumulated

AE hits of the specimens. The ultimate strength and accumulated AE hits were controlled by the corrosion level of the beam specimens. The R2 of the linear graph is 0.5055.

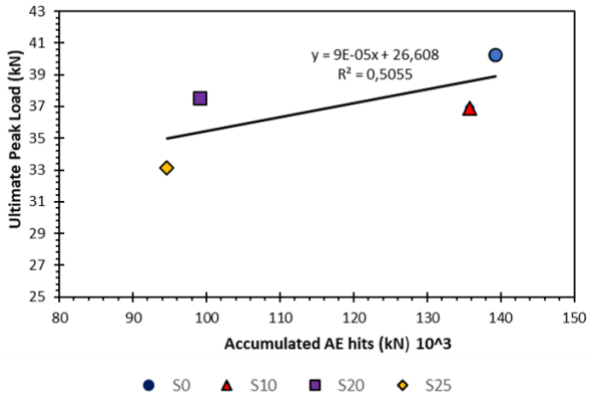

Fig 4. Accumulated AE hits against ultimate peak load of beam specimens

3.2 RA Value and AF

Figure 5 shows RA value vs. AF distribution of the AE data at every 1 kN increment load. The RA value is defined as the ratio of the waveforms rise time to the amplitude, as shown in Equation 6. The AF feature is calculated from the number of thresholds crossing of waveforms divided by duration, as shown in Equation 7. Based on the linear regression for each data group, it is suggested that as the corrosion level becomes higher, there is a collective increase in AF and a decrease in RA value of the beam specimen. It also indicates the beam's transition dominating fracture type, which shifts from shear crack to tensile crack. However, there is a decrease and increase in RA value for the highest corrosion level due to the beam specimen's shear crack progression.

RA value = Rise Time/Amplitude

Average frequency = Counts/Duration

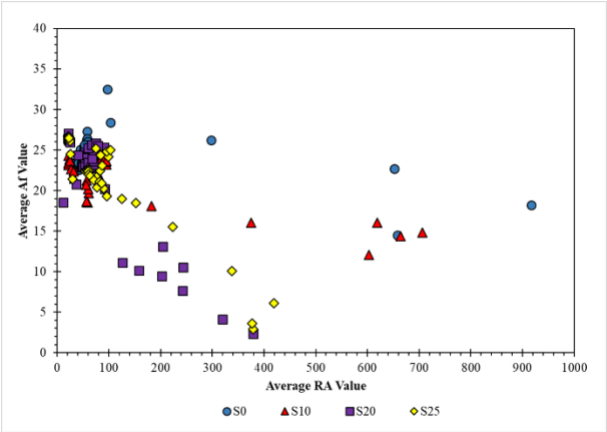

Fig 5. RA value and AF of the concrete beam specimens

3.3 Linear Discriminant Analysis

The description of data used for the classification of LDA is tabulated in Table 1. The data are obtained from the AE parameters, i.e., the RA value of the concrete beam specimens. The data are classified into four classes based on the corrosion levels of the beam specimens. Class 1 is for S0, class 2 is for S10, class 3 is for S20, and class 4 is for S25 beam specimens. For LDA classification data, each beam specimen is classified into four classes based on the LDA class. The LDA was applied to classify RA value data of the beam specimens. Table 1 shows the classification results of LDA. In this study, a system uses validity measures of the test with four classes.

Table 1. Data classifications to test system of LDA

Beam Specimens	Class 1	Class 2	Class 3	Class 4
S0	6472	601	796	18
S10	2746	3272	1116	0
S20	1953	1367	1952	0
S25	1553	698	1070	232

Table 2 shows the classification of AF features of the beam specimens. The table shows that initially, the classified data are predominantly classified as a class they are. The S0 beam specimen failed in the shear crack, the high percentage of S0 beam specimen and Class 1 is assumed as shear crack. Overall, class 1 of the beam specimens are classified as a shear crack, and the class 2 to 4 are classified as tensile crack. Table 2 shows the classification data based on LDA data in terms of the type of crack. The S0 beam specimen dominant as shear crack while for S10, S20, S25 dominant as tensile crack. The type of cracks of the beam specimens is almost the same as the observations. More studies will be required to examine further the reliability of the LDA using other AE parameters.

Table 2. Type of cracks classification based on LDA

Beam Specimens	Shear Cracks (%)	Tensile Cracks (%)
S0	82.06	27.94
S10	38.50	61.50
S20	37.04	62.96
S25	43.46	56.54

4 Conclusion

Based on the observations of RA value vs. AF distribution of the AE data, it is suggested that as the corrosion level becomes higher, there is a collective increase in AF and a decrease in RA value of the beam specimen. It also indicates the beam's transition dominating fracture type, which shifts from shear crack to tensile crack. The classification data give information in terms of statistical features based on the correlation of the distribution data. Based on the beam specimens' classification of the beam specimens' RA value features, class 1 of the beam specimens are classified as a shear crack, and class 2 to 4 is classified as tensile crack. The S0 beam specimen dominant as shear crack while for S10, S20, S25 dominant as tensile crack. The

type of cracks of the beam specimens is almost the same as the observations. The promising results obtained in the analysis are proposed to classify the fracture type of the corroded specimens. Although the results obtained so far are encouraging, more investigations on theoretical and practical aspects are needed to indicate further the applicability of the corroded specimens' classification based on other AE parameters.

Acknowledgement

This work was supported by the Universitas Muhammadiyah Yogyakarta by providing the financial support for this research. This work was also supported by University of Malaya under Grant No. UM.C/625/1/HIR/MOHE/ENG/54 and No. PG164-2015A.

References

[1] M. Badawi and K. Soudki, "Control of corrosion-induced damage in reinforced concrete beams using carbon fiber-reinforced polymer laminates," *Journal of Composites for Construction*, vol. 9, no. 2, pp. 195-201, 2005.

[2] B. Elsener, C. Andrade, J. Gulikers, R. Polder, and M. Raupach, "Half-cell potential measurements - Potential mapping on reinforced concrete structures," *Materials and Structures*, vol. 36, no. 7, pp. 461-471, 2003.

[3] S. Ahmad, "Reinforcement corrosion in concrete structures, its monitoring and service life prediction - A review," *Cement and Concrete Composites*, vol. 25, no. 4–5, pp. 459-471, 2003.

[4] S. Ahmad, M. A. A. Jibran, A. K. Azad, and M. Maslehuddin, "A Simple and Reliable Setup for Monitoring Corrosion Rate of Steel Rebars in Concrete," *The Scientific World Journal*, vol. 2014, p. 10, 2014.

[5] Y. Yuan and Y. Ji, "Modeling corroded section configuration of steel bar in concrete structure," *Construction and Building Materials*, vol. 23, no. 6, pp. 2461-2466, 2009.

[6] Y. Yuan, Y. Ji, and S. P. Shah, "Comparison of two accelerated corrosion techniques for concrete structures," *ACI Structural Journal*, vol. 104, no. 3, pp. 344-347, 2007.

[7] J. Hugenschmidt, A. Kalogeropoulos, F. Soldovieri, and G. Prisco, "Processing strategies for high-resolution GPR concrete inspections," *NDT & E International*, vol. 43, no. 4, pp. 334-342, 2010.

[8] J. Hugenschmidt and R. Mastrangelo, "GPR inspection of concrete bridges," *Cement and Concrete Composites*, vol. 28, no. 4, pp. 384-392, 2006.

[9] A. Zaki, H. K. Chai, D. G. Aggelis, and N. Alver, "Non-Destructive Evaluation for Corrosion Monitoring in Concrete: A Review and Capability of Acoustic Emission Technique," *Sensors*, vol. 15, no. 8, pp. 19069-19101, 2015.

[10] C. Van Steen, L. Pahlavan, M. Wevers, and E. Verstrynge, "Localisation and characterisation of corrosion damage in reinforced concrete by means of acoustic emission and X-ray computed tomography," *Construction and Building Materials*, vol. 197, pp. 21-29, 2019.

[11] D. Ghosh, R. Kumar, A. Ganguli, and A. Mukherjee, "Nondestructive Evaluation of Rebar Corrosion–Induced Damage in Concrete through Ultrasonic Imaging," *Journal of Materials in Civil Engineering*, vol. 32, no. 10, p. 04020294, 2020.

[12] A. Sharma, S. Sharma, S. Sharma, and A. Mukherjee, "Monitoring invisible corrosion in concrete using a combination of wave propagation techniques," *Cement and Concrete Composites*, vol. 90, pp. 89-99, 2018.

[13] A. Zaki, M. Johari, M. Azmi, W. Hussin, W. M. Aminuddin, and Y. Jusman, "Experimental Assessment of Rebar Corrosion in Concrete Slab Using Ground Penetrating Radar (GPR)," *International Journal of Corrosion*, vol. 2018, 2018.

[14] Y. Kawasaki, S. Wasada, T. Okamoto, and K. Izuno, "Evaluation for RC specimen damaged from rebar corrosion by acoustic emission technique," *Construction and Building Materials,* vol. 67, pp. 157-164, 2014.
[15] A. Zaki, H. K. Chai, A. Behnia, D. G. Aggelis, J. Y. Tan, and Z. Ibrahim, "Monitoring fracture of steel corroded reinforced concrete members under flexure by acoustic emission technique," *Construction and Building Materials,* vol. 136, pp. 609-618, 2017.
[16] K. A. Shahid, N. M. Bunnori, M. A. Megat Johari, M. H. Hassan, and A. Sani, "Assessment of corroded reinforced concrete beams: Cyclic load test and acoustic emission techniques," *Construction and Building Materials,* vol. 233, p. 117291, 2020.
[17] V. Leelalerkiet, T. Shimizu, Y. Tomoda, and M. Ohtsu, "Estimation of corrosion in reinforced concrete by electrochemical techniques and acoustic emission," *Journal of Advanced Concrete Technology,* vol. 3, no. 1, pp. 137-147, 2005.
[18] D. G. Aggelis, E. Tsangouri, and D. Van Hemelrijck, "Influence of propagation distance on cracking and debonding acoustic emissions in externally reinforced concrete beams," *Meccanica,* vol. 50, no. 5, pp. 1167-1175, 2015.
[19] D. G. Aggelis, S. Verbruggen, E. Tsangouri, T. Tysmans, and D. Van Hemelrijck, "Characterization of mechanical performance of concrete beams with external reinforcement by acoustic emission and digital image correlation," *Construction and Building Materials,* vol. 47, no. 0, pp. 1037-1045, 2013.
[20] S. E. Dunn, J. D. Young, W. H. Hartt, and R. P. Brown, "Acoustic emission characterization of corrosion induced damage in reinforced concrete," *Corrosion,* vol. 40, no. 7, pp. 339-343, 1984.
[21] D. J. Yoon, W. J. Weiss, and S. P. Shah, "Assessing damage in corroded reinforced concrete using acoustic emission," *Journal of Engineering Mechanics,* vol. 126, no. 3, pp. 273-283, 2000.
[22] M. Ohtsu, "Prospective applications of AE measurements to infra-dock of concrete structures," *Construction and Building Materials,* vol. 158, pp. 1134-1142, 2018.
[23] R. Goldaran and A. Turer, "Application of acoustic emission for damage classification and assessment of corrosion in pre-stressed concrete pipes," *Measurement,* p. 107855, 2020.
[24] Y. Kawasaki, T. Wakuda, T. Kobarai, and M. Ohtsu, "Corrosion mechanisms in reinforced concrete by acoustic emission," *Construction and Building Materials,* vol. 48, no. 0, pp. 1240-1247, 2013.
[25] G. Nounu, "Reinforced concrete repairs in beams," *Construction and building materials,* vol. 13, no. 4, pp. 195-212, 1999.
[26] C. Fang, K. Lundgren, L. Chen, and C. Zhu, "Corrosion influence on bond in reinforced concrete," *Cement and concrete research,* vol. 34, no. 11, pp. 2159-2167, 2004.
[27] T. A. El Maaddawy and K. A. Soudki, "Effectiveness of impressed current technique to simulate corrosion of steel reinforcement in concrete," *Journal of materials in civil engineering,* vol. 15, no. 1, pp. 41-47, 2003.
[28] Y. Jusman, S.-C. Ng, K. Hasikin, R. Kurnia, N. A. A. Osman, and K. H. Teoh, "A system for detection of cervical precancerous in field emission scanning electron microscope images using texture features," *Journal of Innovative Optical Health Sciences,* vol. 10, no. 02, p. 1650045, 2017.
[29] M. M. Galloway, "Texture analysis using gray level run lengths," *Computer Graphics and Image Processing,* vol. 4, no. 2, pp. 172-179, 1975.
[30] J. S. Weszka, C. R. Dyer, and A. Rosenfeld, "A Comparative Study of Texture Measures for Terrain Classification," *IEEE Transactions on Systems, Man, and Cybernetics,* vol. SMC-6, no. 4, pp. 269-285, 1976.